

Tunable Properties of Surface Plasmon Resonance of Metal Nanospheroid: Graphene Plasmon Interaction

Shivani Bhardwaj¹ · Nilesh Kumar Pathak¹ · Alok Ji¹ · R. Uma¹ · R. P. Sharma¹

Received: 23 November 2015 / Accepted: 9 May 2016 / Published online: 24 May 2016
© Springer Science+Business Media New York 2016

Abstract Graphene plasmonic resonances play a significant role for enhancing the photon absorption inside thin film solar devices. We investigate the field rising at the intersection of graphene physics and plasmonics followed by analytical methods in visible domain. The electromagnetic signature of oblate-shaped silver and gold nanoparticles (smaller size) with graphene-supported silicon substrate are analyzed under the quasi-static approximation. The results show that the magnitude of scattering and surface plasmon resonances depend on the aspect ratio, semi major axis length, and thickness of graphene monolayer. We also analyzed the wavelength-dependent photon absorption spectrum for optimized thickness (1 nm) of graphene monolayer with aspect ratio (0.328) of silver and gold nanoparticles under the AM1.5 solar spectrum.

Keywords Graphene plasmonic interaction · Scattering efficiency · Metal nanospheroid · Graphene monolayer · Surface plasmon resonances

Introduction

Graphene, a two-dimensional (2D) form of carbon called a honeycomb lattice, has its unique optical, electric, magnetic, mechanical, and thermal properties with a multitude of exciting applications that are being actively followed by industry and academia [1, 2]. The optical properties of graphene

exhibit most idiosyncratic due to the linear dispersion relationship between the energy and momentum over a wide range of energy, rather than parabolic [3]. This fact explains the behavior of electrons as mass less Dirac fermions (relativistic particles) that contributes to the graphene's ultrahigh charge carrier mobility $>10^5 \text{ cm}^2 \text{ V}^{-1} \text{ s}^{-1}$ for both holes and electrons at room temperature [2, 4, 5]. Further, graphene also behaves as a gapless semiconductor with direct cones of its band structure which leads to promote the light absorption as well as charge carrier generation across an ultrawide spectral range from the ultraviolet to the terahertz [6]. Such broadband absorption is facilitated to enhance optical extinction spectra of oblate-shaped metal nanoparticles (MNPs) in short wavelength limit (visible region) [7, 8]. Furthermore, the optoelectronic characteristics of graphene can be impressively tuned by doping, controlling chemical potential or external gate voltage, and using plasmonic technique at nanoscale [6, 9]. The above mentioned properties of graphene are highly tunable, and they make graphene a unique and distinguished substitute over other materials used in photonic manipulators such as polarizers [10], capacitor [11], ultrafast lasers [12], modulators [13, 14], transistors [15], photodetectors [16], plasmonic components [17–20], and photovoltaics [9].

The coupling of graphene with plasmonic metals results in a high quantum efficiency cell in which graphene acts as a semiconductor as well as plasmonic material. Graphene has an optical nonlinearity which is a very unusual plasmonic property. The photonics and optics of graphene have been reviewed in many more literatures in a comprehensive manner [6, 9]. Graphene possesses itself an intrinsic plasmon which is fascinatingly different from noble metal plasmon and speaks for the substantial coupling with MNPs having tunable frequency ranges from terahertz to visible [9, 21, 22]. Plasmons are oscillations of electrons in conduction band that are loosely bonded [9]. The frequency-dependent permittivity of metal

✉ Shivani Bhardwaj
sshivanni@gmail.com

¹ Centre for Energy Studies, Indian Institute of Technology, Delhi 110016, India

nanostructure gives necessary condition for the resonance to satisfy and is highly affected by the surrounding media. The permittivity is written using the Drude Lorentz model which is also size dependent and shape dependent [8, 23].

In this work, we have derived the optical constant of graphene that depends on the parameters such as conductivity, thickness, and frequency. Further, graphene plasmon interaction including substrate effects is analyzed in terms of forward scattering (FS) and surface plasmon resonances (SPRs) under quasi-static domain. The tunability of SPR peaks depend on various parameters like aspect ratio (h_y/h_z), semi major axis length (h_z), and thickness of the graphene monolayer (spacer). From literature, it is found that tunability of surface plasmon resonance of oblate-shaped MNPs lies in the wavelength range 800 nm up to 1200 nm [7], and resonant excitation of light by the oblate-shaped spheroid lies in ultraviolet to near visible domain [8]. For this present modeling system, we are interested to increase the number of absorbed photons with the help of small MNPs (due to economically viable) in 400–600-nm wavelength range because in this region solar spectrum has high photon density. Forward scattering efficiency from the oblate-shaped MNPs would increase the photon absorption which improves the overall efficiency of silicon wafer-based solar cells in the presence of graphene monolayer (GML). The optical constants of silver and gold metal used in the present paper have been taken from the literature [23–26].

Formulation of the Basic-Proposed Modal Form

Electronic and Optical Model of Graphene

The optical features of GML have been modeled as infinitesimally thin, local two-sided surface expressed as a complex-valued surface conductivity $\sigma(\omega, \mu_c, \Gamma, T)$ where ω is radian frequency, μ_c is chemical potential, Γ is a phenomenological scattering rate, and T is temperature. The frequency-dependent surface conductivity for graphene can be expressed as a sum of two terms that can be quantitatively described by the well-known Kubo formula [10, 27, 28]

$$\sigma_{2D} = \sigma_{intra}(\omega, \mu_c, \Gamma, T) + \sigma_{inter}(\omega, \mu_c, \Gamma, T) \quad (1)$$

The first term of Eq. (1) is simplified corresponding to the intraband electron-photon scattering and can be written as [28]

$$\begin{aligned} \sigma_{intra}(\omega, \mu_c, \Gamma, T) \\ = -i \frac{e^2 k_B T}{\pi \hbar^2 (\omega - i2\Gamma)} \cdot \left[\frac{\mu_c}{k_B T} + 2 \ln \left(\exp \left(-\frac{\mu_c}{k_B T} \right) + 1 \right) \right]. \quad (2) \end{aligned}$$

The second term of Eq. (1) is simplified corresponding to the interband transition contribution for $K_B T \ll |\mu_c|$ [28] and can be approximately expressed as

$$\sigma_{inter}(\omega, \mu_c, \Gamma, T) = -i \frac{e^2}{4\pi \hbar} \ln \left[\frac{2|\mu_c| - \hbar(\omega - i2\Gamma)}{2|\mu_c| + \hbar(\omega - i2\Gamma)} \right] \quad (3)$$

Where μ_c and Γ are the characteristic values, μ_c lies between 50 and 1000 meV and $\Gamma \leq 1$ meV, and \hbar is the reduced Planck's constant. After clear understanding of conductivity, combining the concepts of ohm's law and Maxwell's equation to find the expression of relative permittivity (ϵ_g) in terms of conductivity as [29, 30].

$$\epsilon_g(\omega) = \epsilon_0 \left(1 + i \frac{\sigma_{2D}(\omega)}{\epsilon_0 \omega d} \right) \quad (4)$$

ϵ_0 is the permittivity of free space and d is the thickness of GML. The incident light propagates along the z direction, and hence the electric field is along x axis which is impinged on hybrid graphene structure. The GML is treated as an ultrathin layer with its optimized thickness [31]. The modeled wavelength-dependent optical constant of graphene with constant value of $\mu_c = 100$ meV at room temperature is shown in Fig. 1 using Eq. (4).

Scattering and Absorption Cross Section of MNPs

The interactions of light with silver NPs including graphene layer as a spacer are analyzed in terms of polarisability. The schematic diagram of our modeling device is shown in Fig. 2 which contains thin MNPs/GML/Si wafer.

The calculation of polarisability has been done by solving Laplace equation under electrostatic approximation, where the particle size is much smaller than the wavelength of incident light [8, 26, 32, 33].

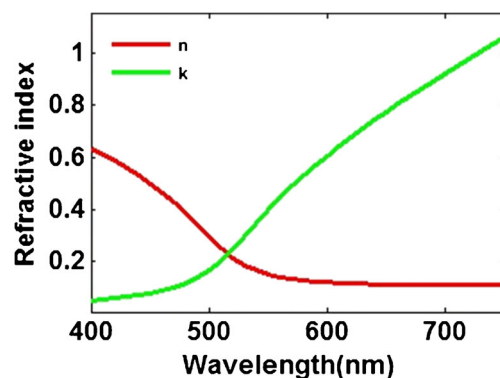
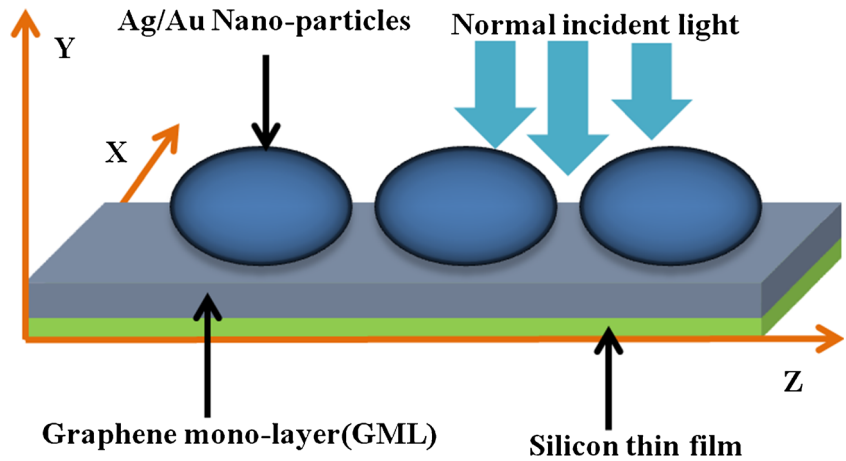


Fig. 1 Variation of the real (n) and imaginary (k) parts of the refractive index of graphene with wavelength at fixed value of graphene thickness 1 nm and chemical potential $\mu_c = 100$ meV

Fig. 2 Schematic diagram of thin film silicon solar cell structure with oblate shape of silver and gold NPs on top of a graphene monolayer (GML)



The optical properties such as scattering and absorption are studied in terms of polarisability tensor having 3×3 dimension as

$$\alpha_{ij} = \begin{bmatrix} \alpha_{||} & 0 & 0 \\ 0 & \alpha_{||} & 0 \\ 0 & 0 & \alpha_{\perp} \end{bmatrix} \quad (5)$$

Where, $\alpha_{||}$ and α_{\perp} represent substrate supported parallel and perpendicular polarisability of metal nanogeometry, respectively, which can be expressed as

$$\alpha_{||,\perp} = \varepsilon_g v_p \frac{(\varepsilon_p - \varepsilon_g)}{\varepsilon_g + (\varepsilon_p - \varepsilon_g) m_{||,\perp}} L_{||,\perp} \quad (6)$$

The symbols ε_g is the dielectric constant of the graphene, v_p is the particle volume, ε_p is the dielectric constant of the silver NPs, ε_d is the dielectric constant of the surrounding environment (air), and

$$L_{||,\perp} = \left[1 + \frac{(\varepsilon_g - \varepsilon_d)(\varepsilon_p - \varepsilon_g)}{3(\varepsilon_g - \varepsilon_d) + (\varepsilon_g + (\varepsilon_p - \varepsilon_g))m_{||,\perp}} U_{||,\perp} \right]^{-1} \quad (7)$$

Where, $U_{||,\perp} = v, 2v; v = h_x h_y h_z (2(d + h_y))^{-3}$ is the normalized parameter depends on chosen NPs size, [33] and h_x, h_y and h_z are the semi axes of oblate-shaped ($h_y < h_x = h_z$) nanospheroid, $m_{||}$ and m_{\perp} are depolarization factors of the NPs along the parallel and perpendicular direction, respectively, which can expressed as

$$m_{||} = \frac{1}{2}(1 - m_{\perp}) \quad (8)$$

$$m_{\perp} = \frac{1 - \xi^2}{\xi^3} (\xi - \arctan \xi) \quad (9)$$

$$\xi = \sqrt{\frac{h_z^2}{h_y^2} - 1} \quad (10)$$

and ξ is the eccentricity of nanospheroid. The random orientation of MNPs are taken into account to study the average scattering and absorption cross section in terms of polarisability as

$$\langle C_{scat} \rangle = \frac{k^4}{6\pi} \left\{ \frac{1}{3} |\alpha_{||}|^2 + \frac{1}{3} |\alpha_{||}|^2 + \frac{1}{3} |\alpha_{\perp}|^2 \right\} \quad (11)$$

$$\langle C_{absp} \rangle = k \text{Im} \left\{ \frac{1}{3} |\alpha_{||}| + \frac{1}{3} |\alpha_{||}| + \frac{1}{3} |\alpha_{\perp}| \right\} \quad (12)$$

$$\langle C_{extn} \rangle = \langle C_{scat} \rangle + \langle C_{absp} \rangle \quad (13)$$

Normalizing all three cross sections to their respective geometrical cross section, we have found the expression of scattering and absorption efficiency as

$$Q_{scat} = \frac{\langle C_{scat} \rangle}{\pi h_x h_z} \quad (14)$$

$$Q_{absp} = \frac{\langle C_{absp} \rangle}{\pi h_x h_z} \quad (15)$$

Photon Absorption

The number of photon absorption (N_{ab}) under the influence of plasmonic effects can be expressed as [7, 34, 35].

$$N_{ab} = [I(\lambda) \times N_p \times C_{scat} + I(\lambda) \times (1 - N_p \times C_{extn}) \times A] \quad (16)$$

Where N_p is the nanoparticle density with 10 % coverage area, and $I(\lambda)$ is the incident light intensity under the AM1.5 solar spectrum [35]. C_{scat} and C_{extn} are the scattering and

extinction cross sections of oblate-shaped nanogeometry. The absorption (A) of photon inside, thin film of silicon, is expressed as

$$A = 1 - \left[R + \frac{RS^2T^2}{1-S^2R^2} + \frac{ST^2}{1-S^2R^2} \right] \quad (17)$$

Where T and R are the transmission and reflection coefficients for Si wafer, respectively, and $s = e^{-\beta z}$, z is silicon wafer thickness ($1 \mu\text{m}$), and β is the absorption coefficient [35] (<http://www.pveducation.org/pvc/drom/appendicies/optical-properties-of-silicon>).

Results and Discussion

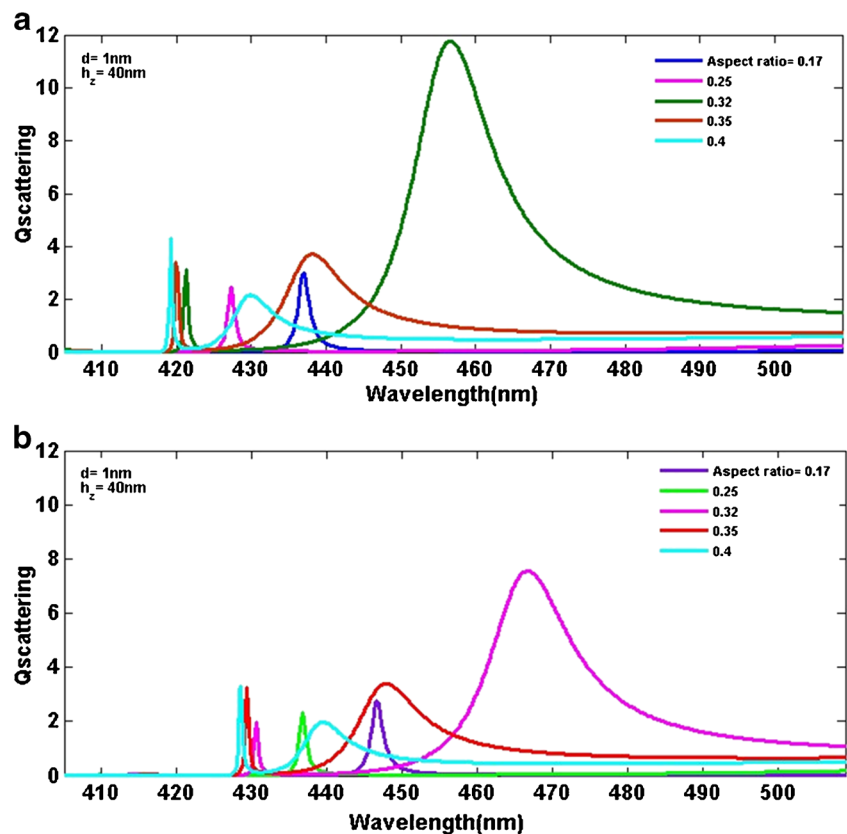
For the absolute light trapping in GML-based thin film silicon cell, forward scattering from the oblate-shaped MNPs is very important which transmits the energy from localized surface plasmons (LSPs) in the form of light. Scattered light after the transmission from GML goes towards the Si wafer and hence the effective path length of light increases. This enhanced path length of light is responsible to improve the absorption of photon in solar cell. The optical signature of MNPs substituted at certain distance from the substrate is analyzed in terms of SPRs. The tunability of these plasmonic resonances depends

on the nanogeometry of surrounding environment and spacer thickness (GML).

Figure 3 shows the wavelength-dependent Q_{scat} spectra of oblate-shaped silver and gold NPs at optimized thickness ($d = 1 \text{ nm}$) of GML with different aspect ratio (ASR) ranges from 0.17 to 0.40, respectively. The oblate-shaped silver and gold NPs are defined as $h_x = h_z = 40 \text{ nm}$ and $h_y = \text{ASR} \times h_z$ where h_x, h_z are semi major axes of spheroid along x and z axes, respectively, h_y is semi minor axis along y axis. As we increase the ASR with constant value of d (spacer thickness) and h_z , SPRs have wide range of tunability in the visible domain of electromagnetic spectrum (400 to 650 nm).

Generally, spheroid shape MNPs support three plasmonic peaks along the three axes separately. Here, we have considered the oblate-shaped MNPs, where two of the three axes are equal and hence only two SPR peaks are observed due to the oscillation of conduction electrons along the two axes of nanoparticle. As we change the axes length or ASR, corresponding SPR changes. In case of smaller ASR, oblate-shaped MNP shows single SPR peak because for smaller ASR; MNP behaves like spherical nature, and hence the oscillation of electrons occurs symmetrically. But for higher ASR, oblate-shaped metal nanospheroid represents dual SPR peaks because the oscillation of electrons becomes axes length dependent. The sensitivity of SPR peak depends on the ASR of chosen nanogeometry, and it gets blue shifted for higher value

Fig. 3 Wavelength-dependent-simulated scattering efficiency: **a** oblate-shaped silver NPs and **b** oblate-shaped gold NPs, at the optimized thickness of GML $d = 1 \text{ nm}$ with various aspect ratio ranges from 0.17–0.40. For oblate-shaped NP, semi major axis length is $h_x = h_z = 40 \text{ nm}$ and semi minor axis length is $h_y = \text{ASR} \times h_z$



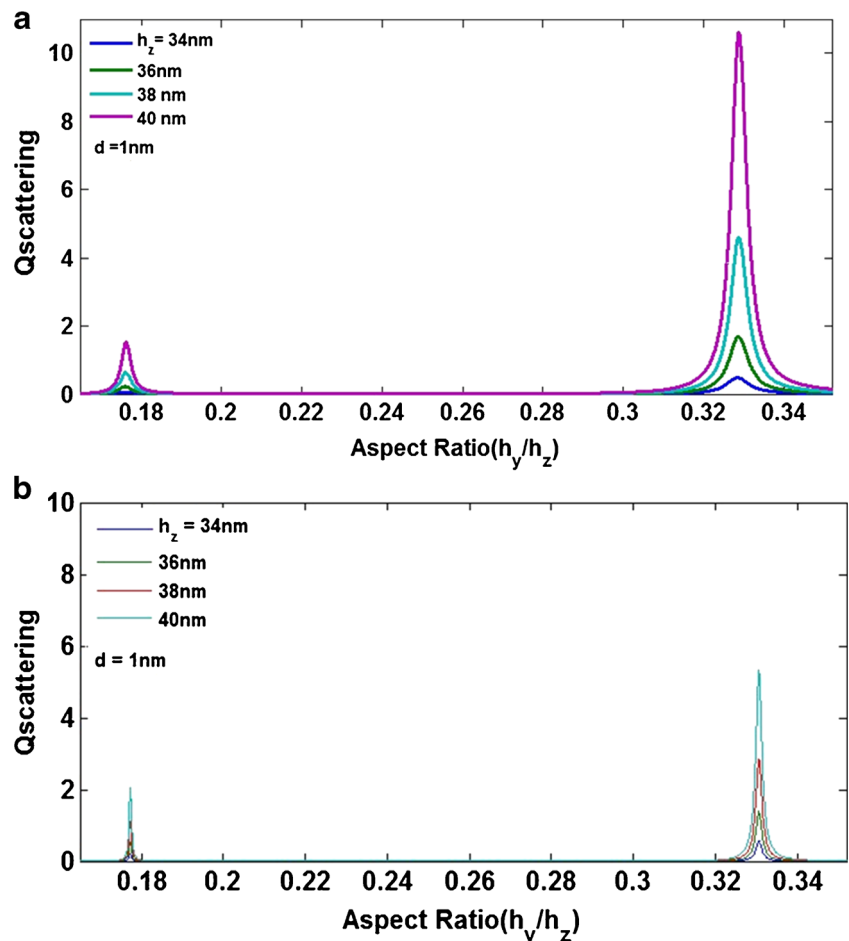
of ASR. For example, out of various ASR at ASR = 0.32, the two different scattering magnitude at different resonant wavelength are observed. From Fig. 3a, we found the narrowband peak at shorter wavelength (421 nm) and the broadband peak at higher wavelength (456 nm) for silver NPs. As in case of gold NPs, we observed the same characteristics of SPR peaks at 431 and 467 nm for narrow and broadband, respectively, as shown in Fig. 3b. The magnitude of Qscattering is higher corresponding to broadband resonances as compared to narrowband amplitude. The narrowband and broadband peaks occur due to the oscillation of conduction electrons along the minor and major axes of the oblate-shaped metal nanospheroid. Individual SPR peak for narrowband as well as broadband have been red shifted (as compare to silver spectrum) for all ASR ranging from 0.17 to 0.4 for gold NPs. This happens due to the combined effects of graphene plasmon interaction which supports high number of free electrons excitation for surface modes at 431 and 467 nm (more dominating broadband) for ASR = 0.32. The difference in broadband resonant peak position between Ag and Au NP is 11 nm, and narrowband peak is nearly 10 nm for ASR = 0.32. From Fig. 3, it can be concluded that, for ASR 0.32, $d = 1$ nm and $h_z = 40$ nm, oblate-shaped silver NPs have higher scattering efficiency

and higher spectral width than gold NPs. This tunability and the spectral broadening of SPR can be utilized to enhance the photon absorption inside graphene-based thin silicon substrate.

Figure 4a shows the scattering efficiency of an oblate-shaped Ag NPs as a function of ASR with different values of semi major axis length ($h_z = 34, 36, 38,$ and 40 nm) at resonance wavelength 456 nm having fixed thickness of GML (TGML) that equals to 1 nm.

However, as the particle size increases, the scattering efficiency also increases consistently; utilizing this property, we can enhance light trapping in thin film Si solar cell [36]. As the semi major axis length increases, we have found double dipole peaks; one lies in lower ASR and other one in higher ASR domain at resonant wavelength 456 nm. The dual resonant peaks observed in the scattering spectrum are due to structural anisotropic effects and collective excitation of the free electrons which is low inside Ag NPs. Optical response of an oblate-shaped Au NPs is plotted in terms of scattering efficiency as a function of ASR, as shown in Fig. 4b. Significant enhancement of this optical response is due to increment of semi major axis length ($h_z = 34, 36, 38,$ and 40 nm) of oblate-shaped Au NPs at optimized value of GML ($d = 1$ nm) and

Fig. 4 Scattering efficiency. **a** oblate silver NPs and **b** oblate gold NPs, (nanospheroid) as a function of ASR with different values of semi major axis length $h_z = 34, 36, 38,$ and 40 nm, at the optimized thickness of graphene monolayer $d = 1$ nm



resonance wavelength 467 nm. In this case, we found dual plasmonic peaks with distinct scattering magnitude in two different regime of ASR. Existence of these weak surface modes due to occurrence of the high multipolar charge distribution and high energy absorbed (high excitation of free electrons) by Au NPs.

From Fig. 4, we also observed that magnitude of $Q_{\text{scattering}}$ is dominated in the higher ASR side as compared to lower ASR, because collective excitation of free electron is higher along semi major axis than semi minor axis. In case of nanospheroid, surface modes are highly dependent on incident electromagnetic signature. Let us now discuss numeric value of $Q_{\text{scattering}}$ of chosen MNPs at optimum value of $h_z=40$ nm, $d=1$ nm, and SPR wavelength 456 nm; we found that the magnitude of $Q_{\text{scattering}}$ is around 1.8 (in lower ASR) and around 10 (in higher ASR) for Ag NPs, while magnitude of $Q_{\text{scattering}}$ is around 2 (in lower ASR) and around 5.3 (in higher ASR) for Au NPs. The entire scattering spectrum has been plotted using Eq. (14). Further, the most important parameter is the TGML (d), which plays a pivot role to study the forward scattering efficiency (FSE) of MNPs.

Figure 5a and b shows the GML thickness-dependent scattering efficiency of oblate-shaped silver and gold NPs, respectively, with fixed ASR=0.328 at $h_z=40$ nm. The magnitude of $Q_{\text{scattering}}$ increases gradually up to the 1-nm GML

thickness and after that it decrease consistently with d . For $d=1$ nm, Q_{scat} is maximum due to the optical sensitivity of GML is high for low values of TGML [37]. In Fig. 6, we have discussed the wavelength-dependent scattering spectra of oblate-shaped Ag and Au NPs with optimized value of ASR=0.328 and $h_z=40$ nm. TGML directly influences the magnitude of $Q_{\text{scattering}}$ and spectral width of surface mode. It is also observed that the tunability of SPR peaks strongly depends on the TGML.

From Fig. 6a, as TGML increases after 0.8 nm, we observed double plasmonic peaks with two different scattering magnitudes. Out of various TGML for Ag NPs, we choose optimized thickness 1 nm where two SPRs are observed at wavelength 436 and 456 nm, respectively. As TGML increase beyond 1 nm, we found double SPR peaks with blue shifted as well as low scattering magnitude. Figure 6b explains sensitivity of the optical response of Au NPs at 1 nm of GML thickness. In this case, double plasmonic peaks are observed at wavelength 446 and 462 nm. As TGML increases from 0.8 to 1.2 nm, characteristic SPR shifts move towards the lower wavelength. It is observed that individual characteristic SPR shifts are also blue shifted for gold NPs with low scattering amplitude [38]. The narrow and broadband peaks highly depend on the thickness of GML. The blue shifted narrowbands corresponding to higher multipole excitation of electric field

Fig. 5 Scattering efficiency. **a** oblate silver NPs and **b** oblate gold NPs as a function of the thickness of graphene monolayer “ d ” at $h_z=40$ nm and ASR = 0.328

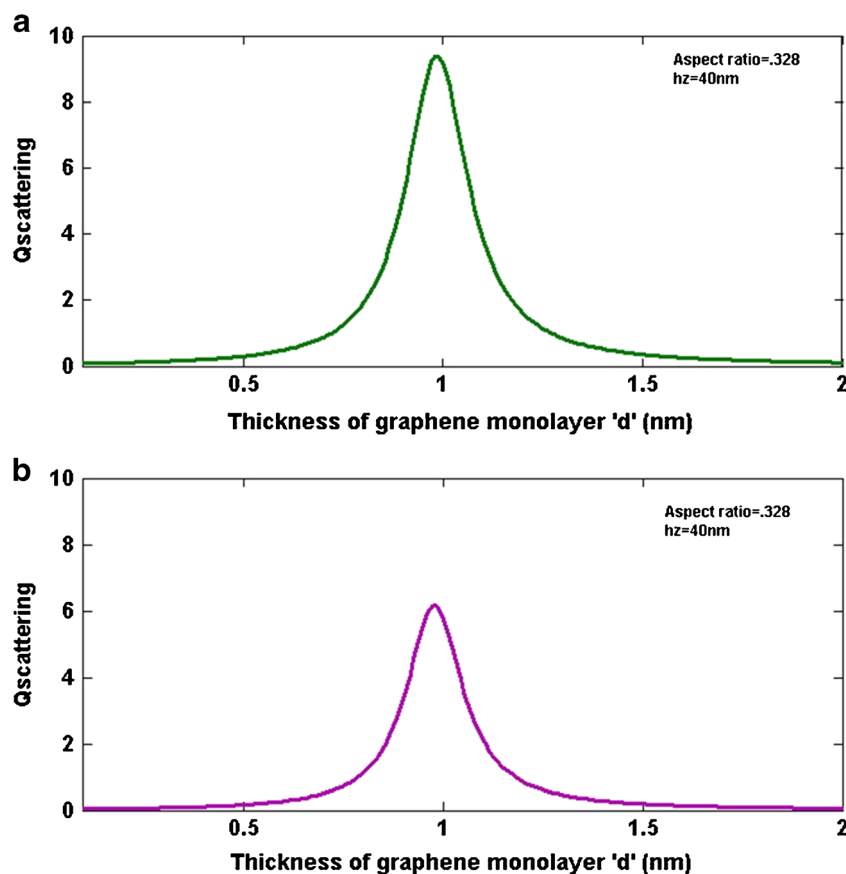
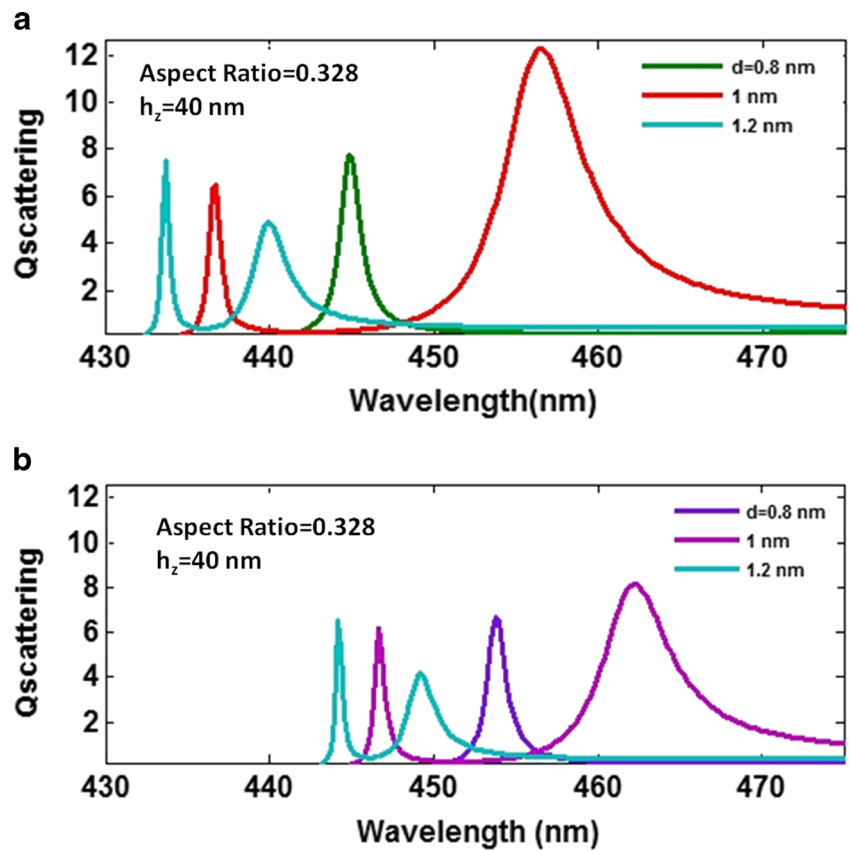


Fig. 6 Wavelength-dependent scattering efficiency of oblate (a) silver NPs and (b) gold NPs, with different values of GML thickness $d=0.8, 1$ and 1.2 nm, $h_z=40$ nm, and $ASR=0.328$

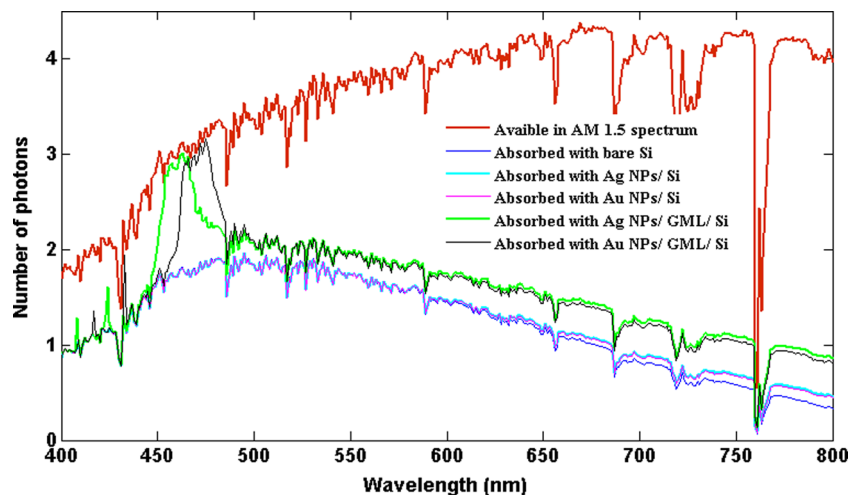


and broadband correspond to dipolar excitation. This higher order multipole excitation exists because of the excitation of free electrons in conduction band which is not homogeneous on the surface of the oblate-shaped MNPs due to eccentricity.

The overall photon absorption inside silicon substrate using graphene plasmonic effects is plotted against the wavelength under the influence of AM1.5 solar spectrum. The red curve is for the available solar spectrum and black and green curves representing the photon absorption for Au/GML/Si and Ag/GML/Si system, respectively. From Fig. 7, it is clear how TGML boosts the photon absorption performance as

compared to bare Si, Ag/Si, and Au/Si systems. We observed that photon absorption spectrum of bare Si, Ag/Si, and Au/Si was coinciding in the wavelength range 400 to 650 nm [7]. Since, there is no appropriate enhancement in photon absorption into Metal/Si thin film. In order to resolve this problem, GML is introduced as a spacer between metal and Si wafers. After introducing the GML, photon absorption capability has been improved in the wavelength range 400 to 800 nm [39]. The enhancement in photon absorption is around 12 % after introducing the GML as spacer in MNPs/GML/Si device which is calculated using Eqs. (16) and (17). This observed

Fig. 7 Absorption of photons in a bare silicon, thin silicon wafer with integrating oblate-shaped Ag and Au NPs, thin silicon wafer with integrating oblate-shaped Ag and Au NPs with GML by integrating oblate-shaped Ag and Au NPs. The selected parameters are $h_z=40$ nm, $d=1$ nm, and $ASR=0.328$



improvement in device (MNPs/GML/Si) is due to high conductivity of graphene (calculated from Eq. (1)). The scattering of light with the MNPs (which are integrated on GML/silicon substrate) enhances the effective path length of light and the collecting excitation of free electron inside thin film of silicon which improves all the characteristics of solar cell that governs by photons. All the photon absorption spectrum is plotted using Eqs. (16) and (17).

Conclusion

We developed an analytical method to study the scattering efficiency of oblate-shaped silver and gold NPs integrated on GML/silicon substrate. The thickness of GML is responsible to tune the SPRs in visible domain. The optical properties of GML basically depend on the thickness of graphene, which comes from electrical property (conductivity) of GML. Further, scattering efficiency has been investigated under the influence of ASR and TGML. Finally, it is concluded that the SPR gets blue shifted with increase in ASR as well as TGML. We have also analyzed that the high scattering efficiency occurs at the optimum value of ASR, major axis length, and TGML, which are responsible for the light trapping and enhance the number of absorbed photons in 400–700-nm wavelength range into Si wafer because in this region the solar spectrum having high photon density. Graphene leads to highly efficient and inexpensive solar cells. Graphene-based plasmonic solar cell forms a coupled resonant system that enables high photon absorption near ultraviolet and visible domain due to scattering and presence of resonant field. These optical devices lay a foundation to future high efficiency with the help of numerical techniques (DDA and FDTD).

Acknowledgments This research is financially supported by MNRE India.

References

- Geim AK, Novoselov KS (2007) The rise of graphene. *Nat Mater* 6: 183–191
- Novoselov KS, Geim AK, Morozov SV, Jiang D, Katsnelson MI, Grigorieva IV, Dubonos SV, Firsov AA (2005) Two dimensional gas of massless Dirac fermions in graphene. *Nature* 438:197–200
- Jablan M, Soljačić M, Buljan H (2013) Plasmons in Graphene: Fundamental Properties and Potential Applications. *Proc IEEE* 101(7)
- Bolotin K, Sikes K, Jiang Z, Klima M, Fudenberg G, Hone J, Kim P, Stormer H (2008) Ultrahigh electron mobility in suspended graphene. *Solid State Commun* 146:351
- Berger C, Song Z, Li X, Wu X, Brown N, Naud C, Mayou D, Li T, Hass J, Marchenkov AN, Conrad EH, First PN, de Heer WA (2006) Electronic confinement and coherence in patterned epitaxial graphene. *Science* 312:1191–1196
- Bonaccorso F, Sun Z, Hasan T, Ferrari AC (2010) Graphene photonics and optoelectronics. *Nat Photonics* 4:611–622
- Ji A, Sharma RP, Kumari A, Pathak NK (2013) Numerical simulation of solar cell plasmonics for small and large metal nano clusters using discrete dipole approximation. *Plasmonics* 9:291–297
- Noguez C (2007) Surface plasmons on metal nanoparticles: the influence of shape and physical environment. *J Phys Chem C* 111(10):3806–3819
- Grigorenko AN, Polini M, Novoselov KS (2012) Graphene plasmonics. *Nat Photonics* 6:749–758
- Bao Q, Zhang H, Wang B, Ni Z, Lim C, Wang Y, Tang D, Loh K (2011) Broadband graphene polarizer. *Nat Photonics* 5:411
- Miller J, Outlaw R, Holloway B (2010) Graphene double-layer capacitor with ac line-filtering performance. *Science* 329:1637
- Sun Z, Hasan T, Torrisi F, Popa D, Privitera G, Wang F, Bonaccorso F, Basko D, Ferrari A (2010) Graphene mode-locked ultrafast laser. *ACS Nano* 4:803–810
- Liu M, Yin X, Ulin-Avila E, Geng B, Zentgraf T, Ju L, Wang F, Zhang X (2011) A graphene-based broadband optical modulator. *Nature* 474:64–67
- Rao S, Heitz J, Roger T, Westerberg N, Faccio D (2014) Coherent control of light interaction with graphene. *Opt Lett* 39:5345–5347
- Engel M, Steiner M, Lombardo A, Ferrari AC, Löhneysen H, Avouris P, Krupke R (2012) Light–matter interaction in a microcavity controlled graphene transistor. *Nat Commun* 3:906
- Gan X, Shiue R, Gao Y, Meric I, Heinz T, Shepard K, Hone J, Assefa S, Englund D (2013) Chip-integrated ultrafast graphene photodetector with high responsivity. *Nat Photonics* 7:883–887
- Jablan M, Buljan H, Soljačić M (2009) Plasmonics in graphene at infrared frequencies. *Phys Rev B* 80:245435
- Abajo F (2014) Graphene plasmonics: challenges and opportunities. *ACS Photonics* 1(3):135–152
- Lu H, Zeng C, Zhang Q, Liu X, Hossain M, Reineck P, Gu M (2015) Graphene-based active slow surface plasmon polaritons. *Sci Rep* 5:8443
- Yu R, Alae R, Lederer F, Rockstuhl C (2014) Manipulating the interaction between localized and delocalized surface plasmon-polaritons in graphene. *Phys Rev B* 90:085409
- Freitag M, Low T, Zhu W, Yan H, Xia F, Avouris P (2013) Photocurrent in graphene harnessed by tunable intrinsic plasmons. *Nat Commun* 4: Article No. 1951
- Echtermeyer TJ, Britnell L, Jasnok PK, Lombardo A, Gorbachev RV, Grigorenko AN, Geim AK, Ferrari AC, Novoselov KS (2011) Strong plasmonic enhancement of photovoltage in graphene. *Nat Commun* 2:Article No. 458
- Kreibig U, Vollmer M (1995) *Optical properties of metal clusters*. Springer, Berlin
- Johnson PB, Christy RW (1972) Optical constants of noble metals. *Phys Rev B* 6:4370
- Palik ED (1985) *Handbook of optical constants of solids*. Academic, Orlando
- Bohren F, Huffman DR (1998) *Absorption and scattering of light by small particles*. Wiley Press, New York
- Zhao B, Zhao JM, Zhang ZM (2014) Enhancement of near-infrared absorption in graphene with metal gratings. *Appl Phys Lett* 105(3): 031905
- Hanson GW (2008) Dyadic Green's functions for an anisotropic, Non-local model of biased graphene. *IEEE Trans Antennas Propag* 56(3):747–757
- Wang B, Zhang X, Yuan X, Teng J (2012) Optical coupling of surface plasmons between graphene sheets. *Appl Phys Lett* 100: 131111
- Chew WC (1999) *Waves and fields in inhomogeneous media*. Wiley-IEEE Press, New York

31. Wang B, Zhang X, García-Vidal F, Yuan X, Teng J (2012) Strong coupling of surface plasmon polaritons in monolayer graphene sheet arrays. *Phys Rev Lett* 109:073901
32. Evlyukhin AB, Bozhevolnyi SI (2005) Surface plasmon polariton scattering by small ellipsoid particles. *Surf Sci* 590:173–180
33. Landau L, Lifshitz E (1960) *Electrodynamics of continuous media*. Pergamon Press, London
34. Green MA, Keevers MJ (1995) Optical properties of intrinsic silicon at 300 K. *Prog Photovolt Res Appl* 3:189–196
35. Atwater HA, Polman A (2010) Plasmonics for improved photovoltaic devices. *Nat Mater* 9:205–213
36. Schmid M, Klenk R, Ch M. Lux-Steiner, Topič M, Krč J (2011) Modeling plasmonic scattering combined with thin-film optics. *Nanotechnology* 22: 025204 10pp
37. Nair RR, Blake P, Grigorenko AN, Novoselov KS, Booth TJ, Stauber T, Peres NMR, Geim AK (2008) Fine structure constant defines visual transparency of graphene. *Science* 320:1308
38. Aslan K, Lakowicz JR, Geddes CD (2005) Plasmon light scattering in biology and medicine: new sensing approaches, visions and perspectives. *Curr Opin Chem Biol: Anal Tech* 9:538–544
39. Fei Z, Gregory O, Andreev O, Bao OW, Zhang LM, McLeod AS, Wang C, Stewart MK, Zhao Z, Dominguez G, Thieme M, Fogler MM, Tauber MJ, C-Neto AH, Lau CN, Keilmann F, Basov DN (2011) Infrared nanoscopy of Dirac plasmons at the graphene SiO₂ interface. *Nano Lett* 11:4701–4705